

Real-time volumetric lipid imaging in vivo by intravascular photoacoustics at 20 frames per second

MIN WU,¹ GEERT SPRINGELING,² MATIJA LOVRAK,³ FRITS MASTIK,¹
SOPHINESE ISKANDER-RIZK,¹ TIANSHI WANG,¹ HELEEN M. M. VAN
BEUSEKOM,¹ A. F. W. VAN DER STEEN,^{1,4,5} AND GIJS VAN SOEST^{1,*}

¹Department of Biomedical Engineering, Thorax Center, Erasmus University Medical Center, PO Box 2040, 3000 CA Rotterdam, The Netherlands

²Department of Experimental Medical Instrumentation, Erasmus University Medical Center PO Box 2040, 3000 CA Rotterdam, The Netherlands

³Department of Chemical Engineering, Delft University of Technology, van der Maasweg 9, 2629 HZ Delft, The Netherlands

⁴Department of Imaging Science and Technology, Delft University of Technology, Lorentzweg 1, 2628 CJ Delft, The Netherlands

⁵Shenzhen Institutes of Advanced Technology, Chinese Academy of Sciences, 518055 Shenzhen, China
[*g.vansoest@erasmusmc.nl](mailto:g.vansoest@erasmusmc.nl)

Abstract: Lipid deposition can be assessed with combined intravascular photoacoustic/ultrasound (IVPA/US) imaging. To date, the clinical translation of IVPA/US imaging has been stalled by a low imaging speed and catheter complexity. In this paper, we demonstrate imaging of lipid targets in swine coronary arteries in vivo, at a clinically useful frame rate of 20 s⁻¹. We confirmed image contrast for atherosclerotic plaque in human samples ex vivo. The system is on a mobile platform and provides real-time data visualization during acquisition. We achieved an IVPA signal-to-noise ratio of 20 dB. These data show that clinical translation of IVPA is possible in principle.

© 2017 Optical Society of America

OCIS codes: (110.0110) Imaging systems; (110.5120) Photoacoustic imaging.

References and links

1. J.-M. Yang, K. Maslov, H.-C. Yang, Q. Zhou, K. K. Shung, and L. V. Wang, "Photoacoustic endoscopy," *Opt. Lett.* **34**(10), 1591–1593 (2009).
2. E. Falk, P. K. Shah, and V. Fuster, "Coronary plaque disruption," *Circulation* **92**(3), 657–671 (1995).
3. J. A. Schaar, J. E. Muller, E. Falk, R. Virmani, V. Fuster, P. W. Serruys, A. Colombo, C. Stefanadis, S. Ward Casscells, P. R. Moreno, A. Maseri, and A. F. W. van der Steen, "Terminology for high-risk and vulnerable coronary artery plaques. Report of a meeting on the vulnerable plaque," *Eur. Heart J.* **25**(12), 1077–1082 (2004).
4. J. A. Schaar, A. F. van der Steen, F. Mastik, R. A. Baldewsing, and P. W. Serruys, "Intravascular palpography for vulnerable plaque assessment," *J. Am. Coll. Cardiol.* **47**(8 Suppl), C86–C91 (2006).
5. G. van Soest, A. F. van der Steen, and E. Regar, "Autofluorescence: A new NIR on the block," *JACC Cardiovasc. Imaging* **9**(11), 1315–1317 (2016).
6. G. J. Tearney, E. Regar, T. Akasaka, T. Adriaenssens, P. Barlis, H. G. Bezerra, B. Bouma, N. Bruining, J. M. Cho, S. Chowdhary, M. A. Costa, R. de Silva, J. Dijkstra, C. Di Mario, D. Dudek, E. Falk, M. D. Feldman, P. Fitzgerald, H. M. Garcia-Garcia, N. Gonzalo, J. F. Granada, G. Guagliumi, N. R. Holm, Y. Honda, F. Ikeno, M. Kawasaki, J. Kochman, L. Koltowski, T. Kubo, T. Kume, H. Kyono, C. C. S. Lam, G. Lamouche, D. P. Lee, M. B. Leon, A. Maehara, O. Manfrini, G. S. Mintz, K. Mizuno, M. A. Morel, S. Nadkarni, H. Okura, H. Otake, A. Pietrasik, F. Prati, L. Räber, M. D. Radu, J. Rieber, M. Riga, A. Rollins, M. Rosenberg, V. Sirbu, P. W. Serruys, K. Shimada, T. Shinke, J. Shite, E. Siegel, S. Sonoda, M. Suter, S. Takarada, A. Tanaka, M. Terashima, T. Thim, S. Uemura, G. J. Ughi, H. M. van Beusekom, A. F. van der Steen, G. A. van Es, G. van Soest, R. Virmani, S. Waxman, N. J. Weissman, and G. Weisz; International Working Group for Intravascular Optical Coherence Tomography (IWG-IVOCT), "Consensus standards for acquisition, measurement, and reporting of intravascular optical coherence tomography studies: A report from the International Working Group for Intravascular Optical Coherence Tomography Standardization and Validation," *J. Am. Coll. Cardiol.* **59**(12), 1058–1072 (2012).
7. O. Manfrini, E. Mont, O. Leone, E. Arbustini, V. Eusebi, R. Virmani, and R. Bugiardini, "Sources of error and interpretation of plaque morphology by optical coherence tomography," *Am. J. Cardiol.* **98**(2), 156–159 (2006).

8. C. V. Bourantas, F. A. Jaffer, F. J. Gijssen, G. van Soest, S. P. Madden, B. K. Courtney, A. M. Fard, E. Tenekecioglu, Y. Zeng, A. F. W. van der Steen, S. Emelianov, J. Muller, P. H. Stone, L. Marcu, G. J. Tearney, and P. W. Serruys, "Hybrid intravascular imaging: recent advances, technical considerations, and current applications in the study of plaque pathophysiology," *Eur. Heart J.* **97**, ehw097 (2016).
9. G. van Soest, E. Regar, and A. F. van der Steen, "Photonics in cardiovascular medicine," *Nat. Photonics* **9**(10), 626–629 (2015).
10. R. P. Choudhury, V. Fuster, and Z. A. Fayad, "Molecular, cellular and functional imaging of atherothrombosis," *Nat. Rev. Drug Discov.* **3**(11), 913–925 (2004).
11. S. Garg, P. W. Serruys, M. van der Ent, C. Schultz, F. Mastik, G. van Soest, A. F. van der Steen, M. A. Wilder, J. E. Muller, and E. Regar, "First use in patients of a combined near infra-red spectroscopy and intra-vascular ultrasound catheter to identify composition and structure of coronary plaque," *EuroIntervention* **5**(6), 755–756 (2010).
12. K. Jansen, M. Wu, A. F. van der Steen, and G. van Soest, "Lipid detection in atherosclerotic human coronaries by spectroscopic intravascular photoacoustic imaging," *Opt. Express* **21**(18), 21472–21484 (2013).
13. M. Wu, A. F. van der Steen, E. Regar, and G. van Soest, "Intravascular photoacoustic imaging of vulnerable atherosclerotic plaque," *Interventional Cardiol. Rev.* **11**, 120–123 (2016).
14. B. Wang, A. Karpiouk, D. Yeager, J. Amirian, S. Litovsky, R. Smalling, and S. Emelianov, "In vivo Intravascular Ultrasound-guided Photoacoustic Imaging of Lipid in Plaques Using an Animal Model of Atherosclerosis," *Ultrasound Med. Biol.* **38**(12), 2098–2103 (2012).
15. P. Wang, J. R. Rajian, and J.-X. Cheng, "Spectroscopic imaging of deep tissue through photoacoustic detection of molecular vibration," *J. Phys. Chem. Lett.* **4**(13), 2177–2185 (2013).
16. B. Wang, A. Karpiouk, D. Yeager, J. Amirian, S. Litovsky, R. Smalling, and S. Emelianov, "Intravascular photoacoustic imaging of lipid in atherosclerotic plaques in the presence of luminal blood," *Opt. Lett.* **37**(7), 1244–1246 (2012).
17. B. Wang, J. L. Su, J. Amirian, S. H. Litovsky, R. Smalling, and S. Emelianov, "Detection of lipid in atherosclerotic vessels using ultrasound-guided spectroscopic intravascular photoacoustic imaging," *Opt. Express* **18**(5), 4889–4897 (2010).
18. K. Jansen, M. Wu, A. F. van der Steen, and G. van Soest, "Photoacoustic imaging of human coronary atherosclerosis in two spectral bands," *Photoacoustics* **2**(1), 12–20 (2014).
19. K. Jansen, A. F. van der Steen, M. Wu, H. M. van Beusekom, G. Springeling, X. Li, Q. Zhou, K. K. Shung, D. P. de Kleijn, and G. van Soest, "Spectroscopic intravascular photoacoustic imaging of lipids in atherosclerosis," *J. Biomed. Opt.* **19**(2), 026006 (2014).
20. M. Wu, K. Jansen, A. F. van der Steen, and G. van Soest, "Specific imaging of atherosclerotic plaque lipids with two-wavelength intravascular photoacoustics," *Biomed. Opt. Express* **6**(9), 3276–3286 (2015).
21. P. Wang, T. Ma, M. N. Slipchenko, S. Liang, J. Hui, K. K. Shung, S. Roy, M. Sturek, Q. Zhou, Z. Chen, and J. X. Cheng, "High-speed intravascular photoacoustic imaging of lipid-laden atherosclerotic plaque enabled by a 2-kHz barium nitrite raman laser," *Sci. Rep.* **4**, 6889 (2014).
22. J. Hui, Q. Yu, T. Ma, P. Wang, Y. Cao, R. S. Bruning, Y. Qu, Z. Chen, Q. Zhou, M. Sturek, J. X. Cheng, and W. Chen, "High-speed intravascular photoacoustic imaging at 1.7 μm with a KTP-based OPO," *Biomed. Opt. Express* **6**(11), 4557–4566 (2015).
23. Z. Piao, T. Ma, J. Li, M. T. Wiedmann, S. Huang, M. Yu, K. Kirk Shung, Q. Zhou, C.-S. Kim, and Z. Chen, "High speed intravascular photoacoustic imaging with fast optical parametric oscillator laser at 1.7 μm ," *Appl. Phys. Lett.* **107**(8), 083701 (2015).
24. D. VanderLaan, A. Karpiouk, D. Yeager, and S. Emelianov, "Real-time intravascular ultrasound and photoacoustic imaging," *IEEE Trans. Ultrason. Ferroelectr. Freq.* (posted 15 December 2016; in press).
25. J. Li, T. Ma, D. Mohar, E. Steward, M. Yu, Z. Piao, Y. He, K. K. Shung, Q. Zhou, P. M. Patel, and Z. Chen, "Ultrafast optical-ultrasonic system and miniaturized catheter for imaging and characterizing atherosclerotic plaques in vivo," *Sci. Rep.* **5**, 18406 (2015).
26. K. S. Rathod, S. M. Hamshere, D. A. Jones, and A. Mathur, "Intravascular ultrasound versus optical coherence tomography for coronary artery imaging—Apples and oranges," *Interventional Cardiology Review* **10**(1), 8–15 (2015).
27. M. Wu, K. Jansen, G. Springeling, A. F. van der Steen, and G. van Soest, "Impact of device geometry on the imaging characteristics of an intravascular photoacoustic catheter," *Appl. Opt.* **53**(34), 8131–8139 (2014).
28. K. Y. E. Leung, R. A. Baldewsing, F. Mastik, J. A. Schaar, A. Gisolf, and A. F. W. van der Steen, "Motion compensation for intravascular ultrasound palpography," *IEEE Trans. Ultrason. Ferroelectr. Freq. Control* **53**(7), 1269–1280 (2006).
29. W. J. van der Giessen, O. Sorop, P. W. Serruys, I. Peters-Krabbendam, and H. M. van Beusekom, "Lowering the dose of sirolimus, released from a nonpolymeric hydroxyapatite coated coronary stent, reduces signs of delayed healing," *JACC Cardiovasc. Interv.* **2**(4), 284–290 (2009).
30. J. C. Garber, R. W. Barbee, J. T. Bielitzki, L. Clayton, J. Donovan, C. Hendriksen, D. Kohn, N. Lipman, P. Locke, and J. Melcher, "Guide for the care and use of laboratory animals," The National Academic Press, Washington DC **8**, 220 (2011).
31. Y. Li, X. Gong, C. Liu, R. Lin, W. Hau, X. Bai, and L. Song, "High-speed intravascular spectroscopic photoacoustic imaging at 1000 A-lines per second with a 0.9-mm diameter catheter," *J. Biomed. Opt.* **20**(6), 065006 (2015).

32. X. Bai, X. Gong, W. Hau, R. Lin, J. Zheng, C. Liu, C. Zeng, X. Zou, H. Zheng, and L. Song, "Intravascular optical-resolution photoacoustic tomography with a 1.1 mm diameter catheter," *PLoS One* **9**(3), e92463 (2014).
33. M. Lovrak, D. Gruzdytė, M. Wu, J. van Esch, V. van Steijn, and H. M. van Beusekom, "Implantable artificial plaque as an alternative to atherosclerotic animal models to study stent based drug delivery and other transport phenomena in atherosclerotic plaque," (in preparation).
34. Y. Cao, J. Hui, A. Kole, P. Wang, Q. Yu, W. Chen, M. Sturek, and J.-X. Cheng, "High-sensitivity intravascular photoacoustic imaging of lipid-laden plaque with a collinear catheter design," *Sci. Rep.* **6**, 25236 (2016).
35. H. Yabumoto, Y. Sakane, M. Ono, H. Sato, Y. Kuwana, I. Matsukura, J. Kobayashi, N. Kawakami, M. Hikita, and F. Yamamoto, "Perfluoropolymer waveguide with low loss in wide wavelength range," *Reports of the Research Laboratory, Asahi Glass* **54**, 49–52 (2004).
36. V. Daeichin, M. Wu, N. De Jong, A. F. W. van der Steen, and G. van Soest, "Frequency Analysis of the Photoacoustic Signal Generated by Coronary Atherosclerotic Plaque," *Ultrasound Med. Biol.* **42**(8), 2017–2025 (2016).
37. N. G. Horton, K. Wang, D. Kobat, C. G. Clark, F. W. Wise, C. B. Schaffer, and C. Xu, "In vivo three-photon microscopy of subcortical structures within an intact mouse brain," *Nat. Photonics* **7**(3), 205–209 (2013).

1. Introduction

Cardiovascular diseases (CVDs) are the leading cause of death worldwide. In 2012, 17.5 million people died from CVDs, representing 31% of all the global deaths. Particularly, 42% of these CVD deaths are due to coronary artery disease (CAD), which is most often triggered by the rupture of vulnerable atherosclerotic plaque and ensuing thrombosis [1, 2]. A vulnerable plaque is commonly described as a lipid-rich necrotic core, covered by a thin fibrous cap with macrophage infiltration [3]. These plaques have been implicated in worse short-term and long-term outcomes of coronary interventions, as they may destabilize by intracoronary instrumentation during the intervention, or spontaneously at a later stage. The identification of the vulnerable plaque requiring information on the structure and composition of the plaque [4], can have an important role for guiding the diagnosis and treatment of CAD.

All commercially available intravascular imaging modalities can detect one or more of the defining features of a vulnerable plaque, but none provides conclusive identification [5]. Intravascular optical coherence tomography is well positioned for imaging fibrous cap thickness but has insufficient imaging depth to fully visualize the artery wall [6], and tissue characterization requires a high level of user expertise [7]. Intravascular ultrasound (IVUS) can usually see the entire vessel, but lacks resolution and soft tissue type specificity. This has led to the proposal of multimodal imaging strategies [8]. Optical spectroscopies are ideal for discriminating between tissue types, capitalizing on specific absorption features [9, 10]. IVUS has been combined recently with near-infrared spectroscopy (NIRS), which provides information about the presence of lipid-core plaque, but still is unable to measure its depth relative to the lumen border [11].

Combined intravascular photoacoustic (IVPA) and IVUS imaging is emerging as a promising technology for localization, characterization and quantification of coronary atherosclerotic plaque lipids. IVPA imaging, generating ultrasound signal by the absorption of a short laser pulse in the tissue, is capable of imaging the composition of the artery wall with an adequate imaging depth and resolution based on the optical absorption contrast between different tissues [12, 13]. Tissue contrast in IVPA can be chosen by tuning the excitation wavelength to a specific absorption band of the imaging target. We target atherosclerotic plaque lipid, the most prevalent marker for identifying vulnerable plaques, by choosing an excitation wavelength that excites a PA signal from lipids [12, 14–17], and ideally from atherosclerotic lipids alone [18–20]. Its co-registered IVUS image provides the complementary structure information of the artery wall. Although IVPA/US imaging potentially offers valuable information for assessment of plaque vulnerability, the slow imaging speed and the difficulty in design and fabrication of a miniature flexible catheter have presented as major challenges for translation of IVPA/US imaging into an in vivo or clinical application. An intensive research effort is ongoing towards the further development of IVPA/US imaging systems. Imaging speed is primarily limited by laser pulse rate: with the introduction of 500 Hz to 2 kHz repetition rate laser systems, operating at the wavelengths of

lipid absorption peaks near 1.2 μm or 1.7 μm , the IVPA/US lipid imaging speed has recently increased to about 1 frame per second (fps) [21–23]. Use of a more conventional laser wavelength facilitates speed but offers limited biological image contrast [24].

The routine for intravascular imaging is to perform a pullback while acquiring a series of cross-sectional images, which together form a volume scan. If using the closest relative, IVUS imaging, as a reference, scanning a vessel with a pullback speed of 0.5–1 mm/s and a frame rate of 20–50 fps is required for IVPA imaging. In this paper, we demonstrate an IVPA/US system with a 1.3 mm outer diameter flexible catheter, imaging coronary lipids at the speed of 20 fps, comparable to the speed of a conventional commercial IVUS system [25, 26]. This frame rate is the minimum usable acquisition speed for in vivo volumetric (pullback) imaging, if adequate sampling is required in the presence of cardiac motion. We demonstrate the imaging performance in vivo in a healthy swine model with an introduced lipid target, and on a human atherosclerotic coronary artery sample ex-vivo.

2. Methods and materials

2.1 IVPA/US image acquisition and real-time visualization

The schematic of the high-speed IVPA/US imaging system is shown in Fig. 1. The laser source in the system (FQ-OPO, Elforlight Ltd, Daventry, UK) is a periodically-poled LiNbO₃ OPO pumped by a pulsed Nd:YAG laser, which in turn is pumped by a CW diode. The laser pulse duration is approximately 10 ns, the maximum output pulse energy of the laser is 80 $\mu\text{J}/\text{pulse}$ and the pulse repetition rate is of 5 kHz. The tuning range of the laser is from 1700 to 1750 nm. The laser output is coupled into a multimode optical fiber with a core diameter of 100 μm and connected to the 1.3 mm IVPA/US catheter through an optical rotary joint (Princeton, Hamilton, NJ, USA) and an electrical slip ring (LPT025, JINPAT Electronics, Shenzhen, China) inside the scanning stage. The IVPA/US catheter is based on the design we previously described in [27], consisting of a 100 μm diameter angle polished fiber (angled at 34 degree, low OH, Pioneer Optics, USA), an ultrasound transducer element (40 MHz central frequency, 50% bandwidth, Blatek, USA), a tip assembly made from polyether ether ketone (PEEK), a metal torque coil and a 1.3 mm outer diameter polyethylene (PE) sheath. An ultrasound pulser (AVL-2-PS-P, Avtech Electrosystems Ltd, New York, NY, USA) is used to transmit 80 V amplitude pulses for pulse-echo imaging. A pulse/delay generator (BNC model 575, Berkeley Nucleonics Corporation, San Rafael, CA, USA) provided timing and triggering signals to the laser, digitizer and the ultrasound pulser. The time delay between the PA and US signal is 10 μs . The received data were 43 dB amplified (AU1263, MITEQ, Long Island, NY, USA), band pass filtered (13–60 MHz 5th order Butterworth, custom built), digitized and transferred by a data acquisition card with 14 bits digitization and 400 MS/s sampling rate (PX14400, Signatec, New York, NY, USA) installed in a personal computer (PC).

The data acquisition software was developed in C++ (Microsoft Visual Studio 10) to acquire and display the recorded data in real time. Simple data processing, including decimation, truncation, absolute value, normalization, and scan-conversion to Cartesian coordinates was applied to the acquired data before real-time data display. A video of data acquisition and visualization with the software interface is provided in [Visualization 1](#). Rotation (313518, Maxon motor, Sachseln, Switzerland) and translation motors (143967, Maxon motor, Sachseln, Switzerland) were combined for helical scanning, driving the catheter rotation at 1200 rpm and pullback at 0.1~1 mm/s. One cross-sectional image was composed of 250 A-lines and the whole system is capable of IVPA/US imaging at 20 fps. All the devices were placed in a portable trolley for easy transportation.

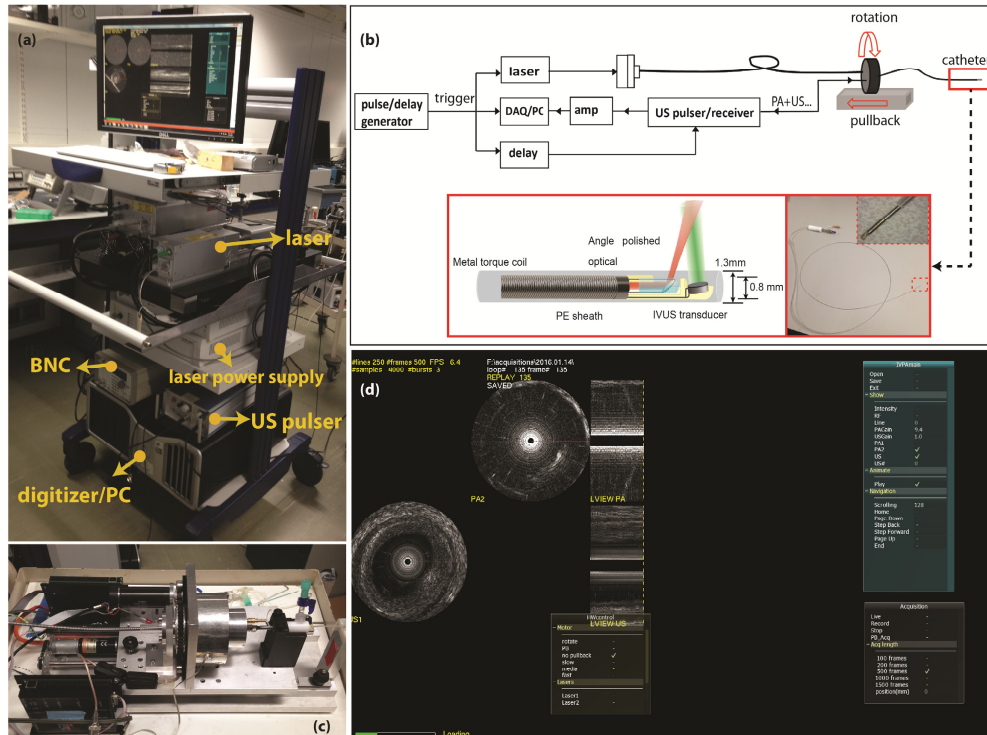


Fig. 1. (a) Photo of the mobile IVPA/US system. (b) Schematic of the IVPA/IVUS imaging system composition and illustration of the IVPA catheter components. (c) Photo of the pullback unit. (d) Data acquiring and display with the homemade software interface on a human coronary artery sample ex vivo (Visualization 1).

2.2 Data processing

Further signal processing on the data was performed in Matlab (R2016a; The Mathworks, Natick, MA, USA) offline. All received PA and US data were decimated, digitally band pass filtered from 10 to 60 MHz, envelope filtered, median filtered, denoised, and converted for display as in our previous work [12]. In the in vivo data, we noticed image wobble in the pullback due to variations in tip rotation speed, possibly related to cardiac motion. We applied a global rotational block matching correction based on the correlation of subsequent IVUS frames [28]. After this motion correction, we enhanced the PA signal to noise ratio (SNR) by averaging each A-line in a 3×2 (lines \times frames) averaging kernel. For instance, the PA signal at i^{th} A-line and j^{th} frame, $P_{i,j}$, was averaged with its two adjacent A-line signals at the same frame $P_{i\pm 1,j}$ and the PA signal at the same three A-lines in the next frame, $P_{i\pm 1,j+1}$.

Furthermore, in vivo imaging is performed through the PE sheath, which attenuates PA signal and introduces strong reflection artifacts. The reflection artifacts are highly correlated throughout the pullback recording. The reference reflection artifact PA signal was constructed from the PA images without the lipid target and was used to cancel the artifacts in images with the lipid target.

2.3 Human coronary artery sample preparation

One artery sample (LAD, 48 year old male) was collected at autopsy from the Department of Pathology of Erasmus Medical Center (MC), after obtaining consent from the relatives. The research protocol was sanctioned by the Medical Ethics Committee of Erasmus MC (MEC-2007-081). The coronary artery was frozen within 2h after autopsy and stored at -80° until

analysis a few months later. Prior to analysis, the artery was thawed and measured within several hours. In the measurement, metal needles were used to fix the artery specimen inside a small container filled with D₂O-saline and register the pullback locations. Figure 2(a) shows a photo of the prepared artery sample for the measurement. The IVPA/US measurement was performed at room temperature at the wavelength of 1720 nm. To maximize the PA SNR, the PE sheath was removed during the measurement. A pullback data set containing 500 frames was acquired at a pullback speed of 0.1mm/s. All the IVPA/IVUS images were non-averaged.

After the measurement, we cut the part of the artery sample imaged, embedded in optimal cutting temperature compound (Tissue-Tek, Sakura Finetek Europe B.V., Alphen a/d Rijn, The Netherlands), and stored it at -80°C until further processing. For histology, we sliced the whole frozen artery block into a series of 10 μm thick sections. Oil Red O (ORO) staining was applied to all these sections to detect lipids.

2.4 *In vivo* IVPA/US imaging in swine coronary lipid model

To further test the imaging system, an *in vivo* IVPA/US experiment was performed on a healthy farmbred (Yorkshire-landrace) swine. The animal was sedated using Zoletil 100 (Virbac Nederland BV, Barneveld, The Netherlands), Sedazine (AST Farma BV, Oudewater, The Netherlands) and Atropine (Pharmachemie BV, Haarlem, The Netherlands), and anesthesia was maintained using pentobarbital (10-15 mg/kg/hr) while connected to a ventilator as described before [29]. The protocol was approved by the Erasmus MC Animal Ethics committee and was performed in accordance with the Guide for Care and Use of Laboratory Animals [30]. Following anesthesia and a surgical cut-down, a sheath was introduced into the carotid artery. Then a guiding catheter was advanced to the right coronary artery (RCA) for stent placement and intravascular imaging. Under guidance of angiography a small piece of pork lard was delivered into the coronary artery to mimic the plaque lesion as described by Lovrak et al. [31]. The pork lard (lipid target) was fixed at its two ends with two small, modified, double-layered stents on the balloon catheter (Pantera Pro 4.0/15; Biotronik SE & Co. KG, Berlin, Germany). Figure 3(a) shows the photo of the lipid rich material with stents mounted on the balloon catheter. To prevent the two stents from being pushed apart while inflating the balloon, we connected them with the black surgical wires.

Then, the IVPA/US catheter was advanced into the RCA with a GuideLiner catheter (6F, Vascular Solutions, Minneapolis, MN, USA). The metal stents and the catheter were radio-opaque, thus, the pullback locations could be easily tracked by X-ray imaging [Fig. 3(b)]. In this way, IVPA/US pullback recording was arranged to cover the lipid target region (the region in between the two stents) at a speed of 0.5mm/s. Each pullback recording contains at least 200 frames. The *in vivo* experiment was also performed at 1720 nm, but unlike the *ex vivo* experiment, it imaged through the PE sheath. During the experiment, we continuously flushed the artery with heavy water-based saline. After the experiment, we sacrificed the pig, cut the artery open and confirmed the presence of the lipid target inside the RCA.

3. Results

3.1 *Ex vivo* IVPA/US imaging of human coronary artery

We imaged a human atherosclerotic plaque specimen, obtained from autopsy. Figure 2 shows the combined IVUS/IVPA data. An atherosclerotic lesion with a variable amount of intraplaque lipid, photographed in its holder in Fig. 2(a), is visualized by IVPA/US. The lipid content increases in the pullback direction, from left to right in Fig. 2(b), appearing from 3 o'clock to 7 o'clock in the 3D reconstruction of the pullback data. Histology validations by Oil Red O lipid stain are shown at two pullback locations, indicated with yellow and blue contours in Fig. 2(b). In the combined IVPA/US images [Fig. 2(c) and 2(e)], the IVPA signal can be clearly appreciated at the corresponding thickened intima region within the artery wall (from 2 o'clock to 7 o'clock). This suggests the presence of a lipid-rich plaque, an

observation that is confirmed by comparison with the histology. The proximal location [Figs. 2(c) and 2(d)] shows a bright IVPA signal corresponding to a dense lipid-laden intima. The more distal location [Figs. 2(e) and 2(f)] exhibits a markedly lower IVPA signal, and a less extensive lipid infiltration on histology.

IVPA achieved full visualization of the lipid-rich lesion throughout the depth of the plaque. The signal-to-noise ratio (SNR) of the PA signal in the plaque region in the image is approximately 20 dB without any averaging, validating the capability of plaque visualization with enough imaging depth by IVPA imaging at 1.7 μm in coronary artery.

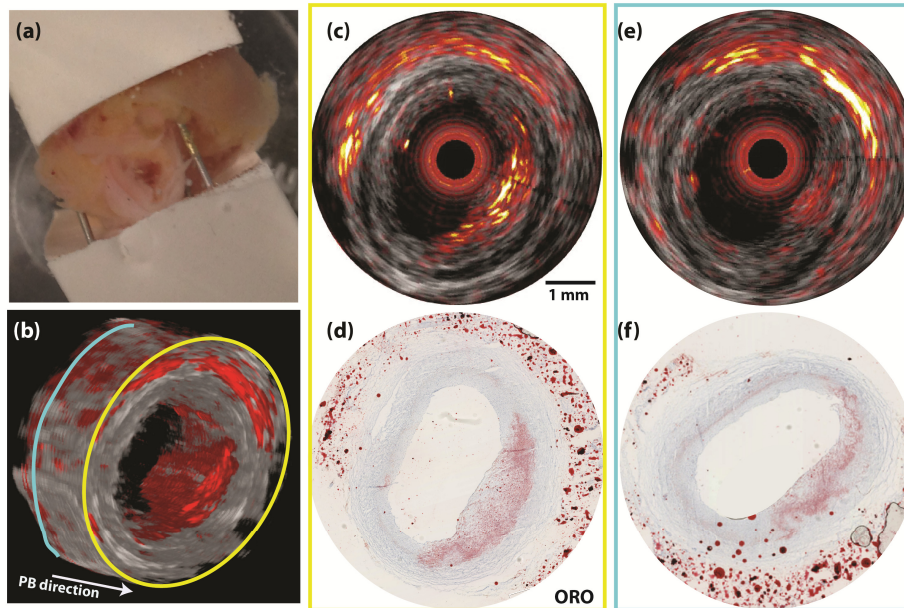


Fig. 2. IVPA/US cross-sectional image of an atherosclerotic human coronary artery. (a) Photo of the human LAD sample fixed inside a holder. (b) 3D reconstruction of the pullback IVPA/US images. (c) Merged IVPA/US image of the plaque at locations with large plaque volume (the location with a yellow contour) and (e) with small plaque volume (the location with a blue contour). (d) and (f) The ORO histology staining at the imaging plane corresponding to images of (c) and (e). The dynamic range is 35 dB in IVUS image and 20 dB in IVPA image. No averaging was applied to IVUS or IVPA data.

3.2 *In vivo* IVPA/US imaging of swine coronary artery

In vivo IVPA/US imaging of a swine coronary artery with an artificial plaque is shown in Fig. 3. A lipid target was introduced into the coronary artery of a healthy animal by attaching a piece of pork fat to a pair of coronary stents and deploying them to attach it to the vessel wall [Fig. 3(a)]. Stents were introduced on a balloon under angiography guidance [Fig. 3(b)]. We acquired a pullback data set using the experimental IVPA/US catheter and system. A longitudinal section of the pullback IVPA/US data containing the lipid target is shown in Fig. 3(c), along with cross-sectional images at two selected pullback locations; one inside the lipid region (yellow line) and the other one outside (blue line). The lipid target can also be seen in the IVUS images as an intraluminal, echogenic object, and this was used to delineate the target by the dotted contour in Figs. 3(c) and 3(d). In the IVPA/US images of the lipid target [Figs. 3(d)-3(f)], a bright PA signal at 6 o'clock to 9 o'clock inside the lumen, generated from the lipid, is clearly observed with an $\text{SNR} \approx 18$ dB (marked with a yellow contour). As a reference, the characteristic PA signal disappears in absence of the lipid target; remaining signal is concentric with the catheter and is attributed to artifacts arising from signal

generation in the catheter sheath. The entire IVPA/US pullback data display (300 frames data) video is shown in [Visualization 2](#).

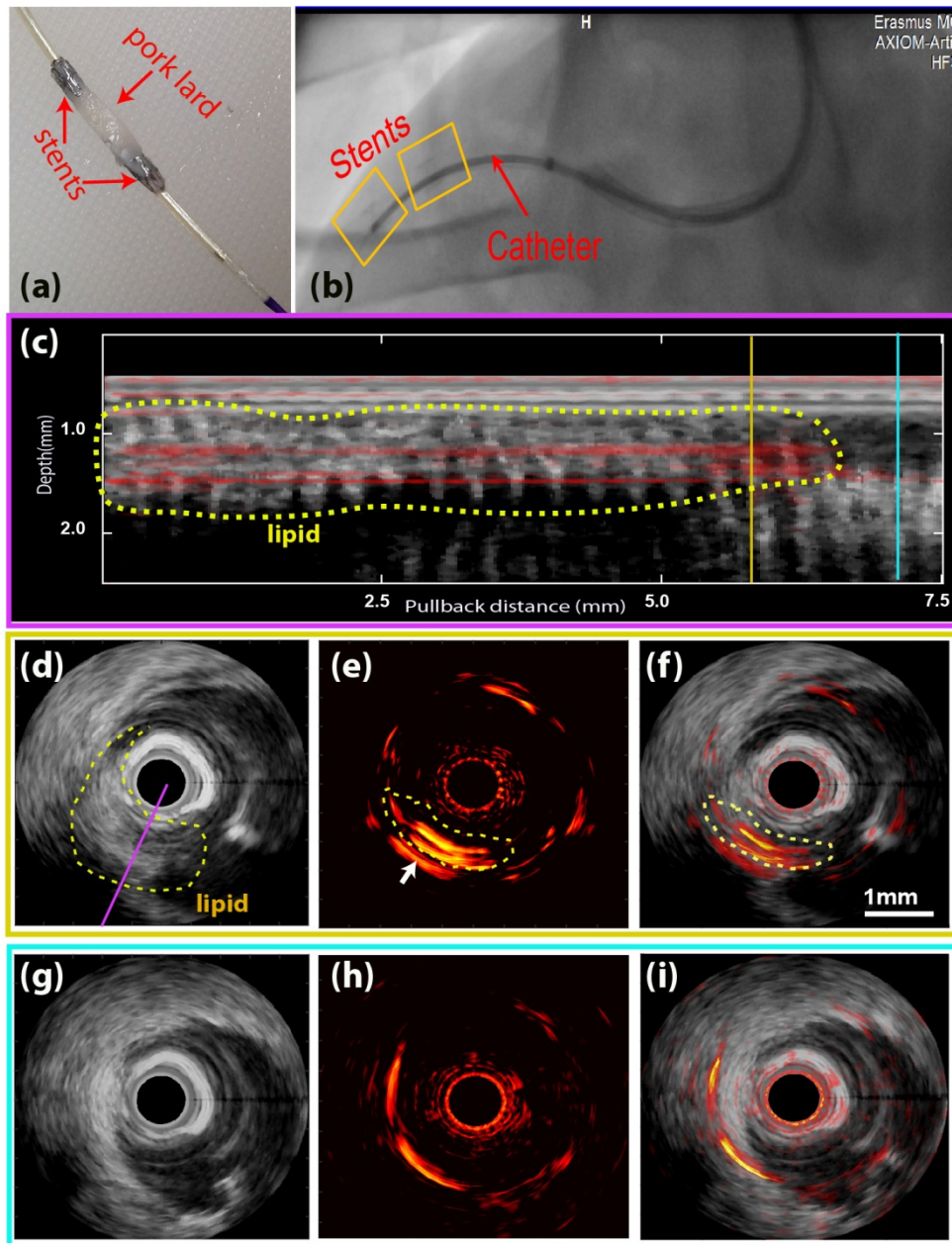


Fig. 3. In vivo IVPA/US imaging result on a swine model. (a) Stents with lipid target mounted on a balloon catheter. (b) X-ray imaging of the pullback location. The stents were inside the yellow boxes and the lipid target located in between the two stents. (c) Longitudinal view of the pullback merged IVPA/US data at an angle intersecting with the lipid object [indicated with a purple line in (d)]. (d,e,f) Cross-sectional IVUS, IVPA, and merged IVPA/US image at the pullback location indicated with a yellow line in (c). (g,h,i) Cross-sectional IVUS, IVPA and merged IVPA/US image at the pullback location indicated with a blue line in (c). The dynamic range is 32 dB for IVUS images and 18 dB for IVPA images; scale bar in (f) applies to all of (d)-(i). The complete pullback data set is available as [Visualization 2](#).

By IVUS, the lipid target appears larger than by IVPA: the IVPA does not detect the entire lipid inclusion. We attribute this to a combination of catheter limitations and image processing: During imaging, the target did not align perfectly with the artery wall, as expected, and as a result was very close to the catheter [Fig. 3(d)]. As described in our previous work [27], an IVPA catheter with a longitudinal beam offset has a low sensitivity to targets that are in close proximity to the transducer due to small optical/acoustic beam overlap. Secondly, imaging artifacts originating from light absorption in the catheter sheath overlapped with the lipid signal. Additional data processing to suppress the artifacts partially suppressed the lipid signal, while some residual artifacts remained, indicated with white arrows in Fig. 3(e). These factors also contribute to more readily apparent motion in the IVUS data.

4. Discussion

In this work, we demonstrated *in vivo* IVPA/US imaging based on a system using a 5 kHz laser with a flexible 1.3 mm catheter, capable of volumetric lipid detection in coronary arteries at 20 frames per second. We validated the imaging system performance on a human coronary artery *ex vivo* and on a swine coronary artery *in vivo*. It is the first *in vivo* IVPA/US imaging in a coronary artery reported to date, acquiring images of coronary lipid in this highly mobile, challenging environment. Our IVPA/US imaging system significantly increased the imaging speed from 1 fps (the fastest imaging speed reported so far for a lipid-imaging IVPA system) to 20 fps [21–23, 31]. The operating parameters of our implementation of this technology match those desired of a clinical imaging system in terms of acquisition speed, operating wavelength, and scan method. The catheter proved to be sufficiently robust for *in vivo* imaging. Further miniaturization of the device is possible and has been demonstrated [31, 32]; the outer diameter could be reduced to < 1 mm with a smaller torque coil and outer sheath.

The IVPA/US system performs acquisition and real-time display of dual-modality data, meaning the data is visualized during imaging at the same rate that it is acquired. This is a key step for usability of IVPA in real-world settings. The image optimizations we performed off-line in the *in vivo* experiments do not require user intervention and could be incorporated straightforwardly in the real-time visualization (inducing a one-frame display delay).

The laser source in our system has a high repetition rate but moderate pulse energy. Partially due to ineffective coupling and scattering at the catheter tip, the optical exposure is less than 0.4 J/cm^2 at $1.7 \mu\text{m}$, which is below the 1 J/cm^2 threshold specified by the ANSI laser safety standard [22]. Despite using a pulse energy which is one order of magnitude lower than that used previously in IVPA/US systems working at $1.7 \mu\text{m}$, the PA SNR achieved in our imaging system was 20 dB, comparable to earlier reports [22, 23]. We used pork lard as a lipid target for *in vivo* imaging, which has a different lipid composition, and thus a slightly different absorption spectrum, compared to lipid-rich plaque [20]. However, at the selected wavelength (1720 nm), both pork lard and plaque generate strong PA signals. An alternative synthetic plaque is being developed, containing the same types of lipids as in plaques to better mimic the plaque lipid signature [33]. This material can be introduced in a similar manner as we did in the present study.

Some challenges clearly remain for the clinical translation of IVPA/US imaging, particularly in the catheter design. In a typical miniature non-collinear IVPA catheter, the offset between the acoustic and optical beams, longitudinally or laterally, leads to a low PA SNR when targets are close to the transducer [27]. Collinear catheter designs do not face this problem, but are more prone to image artefacts resulting from near-field optical absorption [34]. Another difficulty in catheter design is the sheath material, which needs to be transparent for both ultrasound and light (at $1.7 \mu\text{m}$). The polyethylene (PE) material in our current catheter sheath is abundant in C-H bonds as lipids, which makes it a strong absorber at wavelengths providing lipid-specific contrast. A PE sheath absorbs almost half of the PA

excitation energy, leading to a reduction in PA SNR and strong reflection artefacts due to echoes of the sheath-generated signal in IVPA image (Fig. 4). Especially, during the in vivo swine experiment, the artifact from PE sheath appears close to the lipid target, making the PA signal from lipid target a mixture with sheath artifact, which is difficult to completely cancel without losing PA signal originating from tissue. A direct comparison between images with and without sheath shows a similar reduction in PA energy [24].

Attenuation and artifacts affect the quality of in vivo IVPA images compared to the ex vivo IVPA results, collected without sheath. Fluorinated polymers, such as PTFE are an interesting alternative, but tend to have suboptimal mechanical and acoustic properties in their crystalline forms. Fabrication of amorphous fluorinated polymer, such as perfluoro-3-butenyl-vinyl ether (Cytop™), which is flexible and has a 95% transmittance of the light at 1.7 μm [35], in tube form would make these promising materials available for evaluation as catheter sheaths.

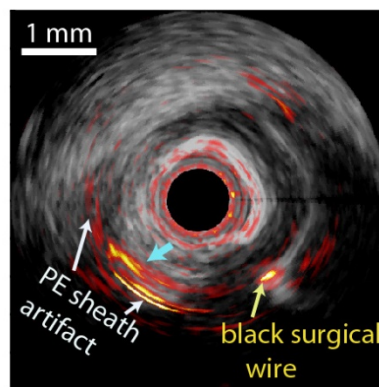


Fig. 4. Merged cross-sectional IVPA/US image of the in vivo result on a swine coronary artery with artificial plaque lesion. White arrow indicates the PE sheath artifact, yellow arrow indicates the black surgical wire and blue arrow indicates the mixture of lipid signal and PE sheath artifact.

Fast and stable laser systems are also essential for translation of IVPA/US imaging to the clinical setting. We need to strike a balance between pulse rate (for speed), pulse energy (SNR), and overall power delivered to the vessel (safety). As 1.7 μm radiation is strongly absorbed by water, it is considered an eye-safe wavelength, which reduces concerns for user safety. We have not seen evidence of laser tissue damage in our human or swine samples, upon deposition of 150 mW of light in the artery. Nevertheless, optically and acoustically efficient designs allow for minimization of the applied laser power while preserving SNR. In recent work [36], we found that 80% of PA power from lipid-rich plaque is at frequencies below 8 MHz, and the PA SNR can be increased up to 20 dB by covering the frequency band below 8 MHz. We experienced >50% optical loss due to fiber coupling and scattering in the tip optics, which is clearly suboptimal. Improved catheter design and functionality may enable IVPA lipid imaging with lower laser pulse energy and output power. Such moderate-output power lasers may prove to be more robust, user-friendly and affordable than the complex OPO system we currently use.

In the present series of experiments, we have chosen to clear blood from the artery for optimizing PA SNR. It is possible to image lipids through blood at 1.7 μm by IVPA imaging [16] due to the relatively small scattering coefficient at infrared wavelengths [37]. H_2O absorption is significant, both in blood and in saline flush, which is why we use D_2O -saline for flushing. Heavy water is non-toxic but expensive, which may present as a limitation going forward.

In summary, we demonstrated volumetric in vivo IVPA/US of lipid in the coronary circulation of a healthy swine. We built an imaging system with a miniature flexible catheter, allowing to image lipid-rich plaque lesions at 20 fps. The system produces good IVPA/US images of lipids with a PA SNR of about 20 dB at the an imaging frame rate that is compatible with comprehensive pullback imaging of coronary plaques.

Funding

Netherlands Organization for Scientific Research (NWO) ZonMW (104003006); Stichting voor de Technische Wetenschappen (STW) (12706).

Acknowledgments

The authors gratefully acknowledge Mr. Keith Oakes from Elforlight Ltd. for the help with the configuration of the laser system. We acknowledge Robert Beurskens from Erasmus MC for his contributions to the development of the IVPA/US imaging system, Ms. Ilona Krabbendam-Peters and Dovile Gruzdyte from Erasmus MC for the help with the in vivo swine experiment and histology.